

Quantitative scheme for full-field polarization rotating fluorescence microscopy using a liquid crystal variable retarder

John F. Lesoine,¹ Ji Youn Lee,^{1,2,a)} Jeffrey R. Krogmeier,^{1,b)} Hyeonggon Kang,¹ Matthew L. Clarke,¹ Robert Chang,¹ Dan L. Sackett,² Ralph Nossal,² and Jeeseong Hwang^{1,c)}

¹*Radiation and Biomolecular Physics Division, National Institute of Standards and Technology, 100 Bureau Drive, Gaithersburg, Maryland 20899, USA*

²*Eunice Kennedy Shriver National Institute of Child Health and Human Development, National Institutes of Health, Bethesda, Maryland 20892, USA*

(Received 26 January 2012; accepted 28 April 2012; published online 16 May 2012)

We present a quantitative scheme for full-field polarization rotating fluorescence microscopy. A quarter-wave plate, in combination with a liquid crystal variable retarder, provides a tunable method to rotate polarization states of light prior to its being coupled into a fluorescence microscope. A calibration of the polarization properties of the incident light is performed in order to correct for elliptical polarization states. This calibration allows the response of the sample to linear polarization states of light to be recovered. Three known polarization states of light can be used to determine the average fluorescent dipole orientations in the presence of a spatially varying dc offset or background polarization-invariant fluorescence signal. To demonstrate the capabilities of this device, we measured a series of full-field fluorescence polarization images from fluorescent analogs incorporated in the lipid membrane of Burkitts lymphoma CA46 cells. The fluorescent lipid-like analogs used in this study are molecules that are labeled by either a DiI (1,1'-Diocetyl 3,3,3',3'-Tetramethylindocarbocyanine) fluorophore in its head group or a Bodipy (4,4-difluoro-4-bora-3a,4a-diaza-s-indacene) molecule in its acyl chain. A spatially varying contrast in the normalized amplitude was observed on the cell surface, where the orientation of the DiI molecules is tangential to the cell membrane. The internally labeled cellular structures showed zero response to changes in linear polarization, and the net linear polarization amplitude for these regions was zero. This instrument provides a low cost calibrated method that may be coupled to existing fluorescence microscopes to perform investigations of cellular processes that involve a change in molecular orientations. [<http://dx.doi.org/10.1063/1.4717682>]

I. INTRODUCTION

Measurement platforms, utilizing techniques from biomedical optics, can provide noninvasive discrimination between diseased and healthy states of both single cells and tissues. Particularly in biomedical imaging, polarization rotating imaging, where different polarizations of light are sequentially used to illuminate a sample, has been demonstrated to differentiate between benign and cancerous tissues in certain types of epithelial cancers or pre-cancers.^{1,2} This discrimination is possible because different cell phenotypes can contain differences in their internal structural anisotropy such as polarized organization of cytoskeletal proteins. The polarized orientations of intracellular or extracellular protein filaments have been measured with polarization-based scattering imaging,³ and the orientations of the absorption dipoles of fluorescent dyes, labeled to tumors, have been observed.⁴ Polarization imaging has also been demonstrated to study the distribution and assembly of lipid molecules and proteins within cells. Heterogeneous lipid distributions in

cell membranes form lipid microdomains, which are likely created by differences in characteristics of lipid molecules such as hydrocarbon chain length and head group charge.⁵ These microdomains induce complex protein distributions and sorting which may play a critical role in determining their functions in the cell membrane.⁶ The lateral organization of proteins and lipids in cellular microdomains has been understood to be a dynamic process, facilitating important cellular functions such as cell signaling transduction, immunological reactions, and the controlled entry and exit of molecules and, e.g., viruses in and out of the cell.⁷

The concept of membrane microdomains has provided new insights into the dynamic relationship between membrane organization and biological functions.⁸ Steady state polarization based imaging has been used to measure the orientational order of fluorescent probes associated with target proteins and lipids in living cell membranes.⁹ This work presents a simple polarization rotating imaging system and its calibration algorithm for imaging the arrangement of lipid molecules in cellular organelles in which the local molecular orientations of lipids are determined by incorporated fluorescent lipid-like probes. Real-time, full-field, and fluorescence polarization rotating microscopy (PROM), employing a liquid crystal variable retarder (LCVR), enables the control of polarization for the excitation light in fluorescence imaging.

Among other probes useful for characterizing subcellular structures involving lipid molecules, fluorescent lipid

^{a)}Present address: Center for Bioanalysis, Division of Metrology for Quality of Life, Korea Research Institute of Standards and Science, Daejeon 305-340, Republic of Korea.

^{b)}Present address: Life Technologies, Inc., 500 Cummings Center, Beverly, Massachusetts 01915, USA.

^{c)}Author to whom correspondence should be addressed. Electronic mail: jch@nist.gov.

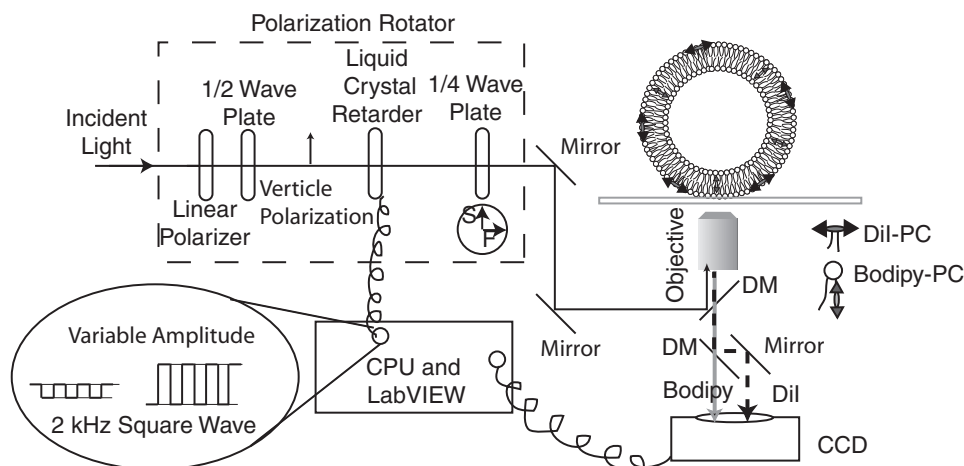


FIG. 1. Experimental schematic of the polarization rotator. S and F denote the slow axis and fast axis of the quarter-wave plate, respectively. Fluorescent lipid analogs, DiI-PC and Bodipy-PC, are shown schematically inserted into a lipid vesicle situated in the focus of the polarization rotation microscope. DiI-PC is assumed to be oriented tangentially to the membrane surface whereas Bodipy-PC is represented perpendicular to the surface. The arrows indicate the directions of the absorption dipoles. DM represents a dichroic mirror.

analogues have been employed as lipid-phase domain labels due to their unique ability to partition into energetically favorable domains in the cell membrane. The analogue with a fluorophore in the head group or in the long acyl chain (i.e., C_{14} or longer) preferentially partitions into the solid phase of the lipid membrane. Those with short acyl chains and unsaturated C–H bonds partition more favorably into the liquid phase. In this study (see Fig. 1), the fluorescence absorption dipole orientations of phosphatidylcholine (PC) lipid molecules conjugated with cationic DiI (DiI $_{C_{16}(3)}$) (D384 Invitrogen, Carlsbad, CA) are probed, using real-time fluorescence polarization microscopy. The DiI dye exhibits a well-defined absorption dipole orientation, thus enabling fluorescence imaging of the dipole orientation using polarization microscopy.¹⁰ Since the DiI moiety in the DiI-PC analogue is attached to the head group and bridges the two acyl chains, its absorption dipole lies along this bridge and is normal to the vector defined along the C_{16} acyl chains. DiI has been shown to report on lipid head-group viscosity through its fluorescence lifetime signal.¹¹ In contrast, the absorption dipole of the Bodipy fluorophore in the Bodipy-PC (D3803 Invitrogen, Carlsbad, CA) analogue is attached to the sn-2-acyl chain by a C_5 alkyl chain. The absorption dipoles of Bodipy lipid analogs, in model dipalmitoylphosphatidylcholine membranes, have been shown to be present in two orthogonal orientations, one being tangential to and the other normal to the membrane surface.¹² Dipole orientations and distributions of DiI-PC and Bodipy-PC, shown tangential and normal, respectively, to the outer surface in a liposome, are indicated in the experimental schematic presented in Fig. 1.

Correspondingly in a cell, the absorption dipole orientations of the DiI dyes, in the DiI-PC construct, are aligned tangential to the membrane surface as a DiI molecule bridging two acyl chains rests on the surface. However, the absorption dipole orientation of the Bodipy dye, which is attached onto one of the two acyl chains in the Bodipy-PC, is determined by a variety of local physical properties such as composi-

tion and packing density (or phase state) of lipids and surface tension which determines the membrane curvature. For instance, membrane packing density is expected to be lower for fluid-phase lipids as opposed to the more densely packed gel-phase lipids.¹³ In a gel-phase domain, acyl chains are expected to be close-packed to result in an ordered alignment of the Bodipy absorption dipole in an orientation perpendicular to the membrane plane. Therefore, the population ratio of surface normal versus tangential Bodipy molecules with increased lateral packing density results in a greater percentage of normal Bodipy orientations relative to the surface of the membrane. Interactions of the acyl chains with cholesterol and membrane proteins will also affect the structural orientations of the acyl chains and attached Bodipy molecules. Thus, Bodipy-PC will provide insight of the local physicochemical properties of the membrane while DiI-PC probes can be used as a reference for the local curvature of the bilayer surface. These lipid-like fluorescent probes may be used as reporters to measure the dynamics of local membrane perturbation (e.g., membrane deformation) by monitoring the change in the absorption dipoles associated with the local fluctuation of the host membrane. Bodipy-PC and DiI-PC molecules have also been used to characterize lipid-phase domain organization.^{14,15} Thus, it should be possible to correlate membrane structural properties to local-phase domains if they are present.

In conventional approaches, polarized light imaging is performed by imaging a sample with the illumination light linearly polarized at a certain polarization orientation angle, followed by imaging the same sample with the light polarized at the other angle perpendicular to the initial polarization. The resulting two images are used to calculate the polarization anisotropy to achieve desired image contrast sensitive to the structural and/or optical anisotropy of the sample. If the sample orientation is held fixed, the Cartesian coordinate system used to define the sample anisotropy has its axes aligned with the perpendicular incident polarizations. A problem general to anisotropy imaging is that the rotational

alignment of this coordinate system is arbitrary. Thus, even though the sample properties can be fixed, the sample anisotropy will be dependent upon the choice of crossed polarizations. In addition, features with orientations rotated to $\pm 45^\circ$ of the incident polarizations cannot be distinguished from isotropic sample regions.¹⁶

In order to produce quantitative images that are independent of the rotation of incident polarization states relative to the sample, a third polarization can be used that is rotated at $\pm 45^\circ$ to the crossed polarizations. The additional information from this third polarization state allows for differential polarization, or anisotropy images to be calculated for incident polarizations rotated at 0° and 90° in addition to 45° and -45° . These two sets of difference images lead to the ability to calculate the rotation invariant degree of linear excitation (DOLE) and the angular projection, θ , of the molecular orientations onto the 2D image plane. The DOLE image map represents the preference of the sample to be excited with linear polarized light rotated at an angle of θ . The rotations associated with the DOLE image signal are found from the corresponding image locations in the angular projection map.

In PROM, the LCVR is incorporated to achieve retardance tunability in the polarized excitation light and combined with a quarter-wave plate to provide linear polarization rotation of the excitation field. The system is coupled to a fluorescence microscope, and the polarization of the incident (or excitation) light is rapidly rotated by changing the peak-to-peak voltage applied to the LCVR. A detailed calibration is used to quantify the components of linear polarization for each applied voltage to the LCVR to correct for the presence of elliptical polarization states of the incident light and for differences in the intensity at the sample for the applied voltages. A series of full-field polarimetric fluorescence images is obtained with a camera synchronized with the controlled polarization of the excitation field. The calibration curve makes an efficient algebraic recovery of linear polarization properties of the sample possible from three separate polarimetric images. The PROM of live Burkitts lymphoma, CA46 cells allows for the measurement of dynamic orientations of the dipoles of DiI molecules in fluorescent DiI-PC lipid analogs tangential to the plasma membrane as their absorption dipole orientations are probed under a constantly rotating polarized excitation field. The dipole orientations of Bodipy molecules in Bodipy-PC lipid analogs were also measured but no net dependence on polarization was observed.¹⁷ The calibration and straightforward algebraic analysis demonstrate that a set of three arbitrary polarizations of light recovers the angular projection (θ) and the DOLE information of the orientations of the dye molecules in DiI-PC or Bodipy-PC incorporated in cellular organelles.

The fluorescence emission of dye-labeled lipid analogs, e.g., head group labeled with different acyl chain lengths or acyl chain labeled at different positions in the chain, can be separated into different color channels as shown in Fig. 1. The separation of these analogs would provide the ability to quantitatively correlate the membrane surface orientations and fluctuations to membrane packing properties. With the potential for the development of real-time data pro-

cessing with a live image display, the PROM may allow for the real-time imaging of local orientations and organizations of cellular lipid molecules with minimal perturbation.

II. MATERIALS AND METHODS

A. Polarization rotator

The quantitative calibration of the microscopic polarization rotation system allows for potential variabilities due to elliptical polarizations of light and for differences in laser power to be corrected for with an algorithmic reconstruction. The first step in the calibration was the proper alignment of the polarizer and half- and quarter-wave plates with respect to the optical axes of the LCVR (Meadowlark Optics, Frederick, CO), as shown schematically in Fig. 1 and described in detail in Ref. 18. The half-wave plate was used to orient the polarization of the incident light at -45° to the fast axis of the LCVR, whereas the slow-axis of the quarter-wave plate that follows the liquid crystal retarder was aligned parallel to the polarization of the incident light. To fine tune the alignment, the amplitude of a square wave, with a frequency of 2 kHz, was swept back and forth between 0 V peak-to-peak and 10 V peak-to-peak using an analog signal generated with LabVIEW program and a signal processing board (PCI 6110 DAQ, National Instruments, Austin, TX). The microscope is operated in a wide-field imaging mode with the incident laser beam focused onto the center of the back aperture of the objective lens. The light passes through a substantially reduced effective numerical aperture, which does not strongly induce spatial variation of its polarization. Hence, the illumination transmitted through the microscope objective can be approximated as a plane wave propagating along the optical axis and, to a very good approximation, the polarization properties of the light exiting the objective are spatially uniform across the imaging field. Other transmission geometries may require special treatment and spatial variation of the polarization properties over the entire imaging field. The light exiting the polarization rotation optics was analyzed with a linear polarizer, set to a random angle in front of a calibrated Si photodetector placed in front of the objective lens.¹⁹ The wave plates were fine-adjusted so that there was a maximum between extinction, where the polarization of the light is perpendicular to the polarizer, and the signal when the polarization of the light is aligned with the analyzing polarizer. Several analyzer angles were checked to ensure proper alignment of the polarization rotator.

The 2 kHz signal with varying peak-to-peak voltages, applied to the LCVR, provides different values of retardation that will result in different angles of linear polarization exiting the quarter-wave plate. Calibration of the polarization angle with the peak-to-peak voltage amplitude applied to the liquid crystal retarder was performed with a custom written LabVIEW program. The calibrated photodetector and polarization analyzer were placed on an Olympus IX81 inverted microscope at the focus of an oil immersion objective (1.45NA, PlanApo). This quantifies the polarization characteristics of the light incident at the sample. The peak-to-peak voltage applied to the liquid crystal rotator was swept between

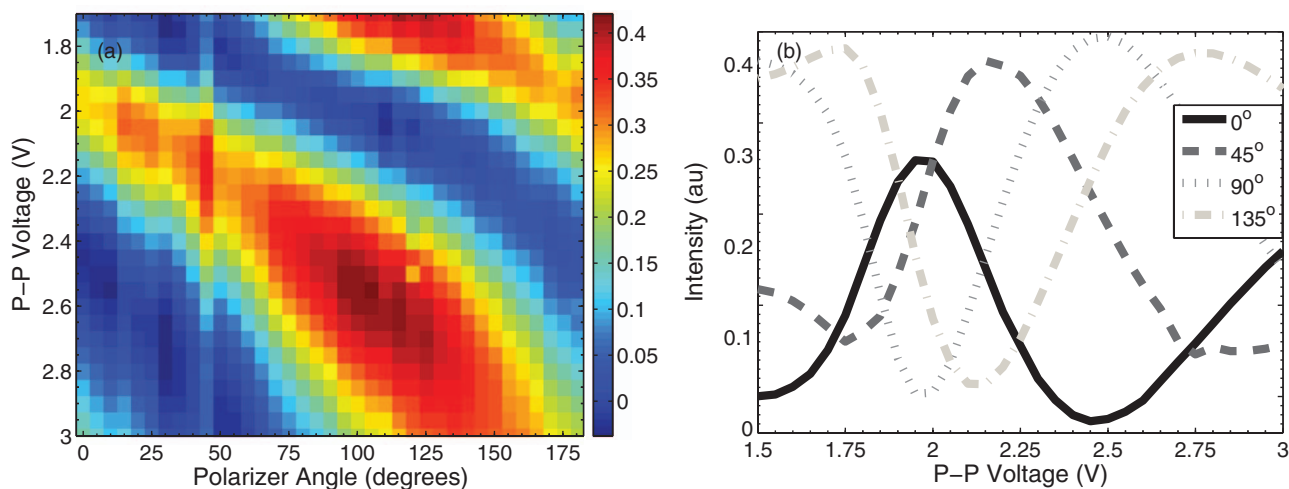


FIG. 2. Calibration data of polarization angle vs. applied peak-to-peak voltage to the LCVR. (a) A calibration map of peak-to-peak voltage vs. polarizer angle was used to determine the linear polarization output of the polarization rotator as a function of the applied voltage. This calibration map can be used to calculate the Stokes parameters for the incident light. (b) Four cross sections of intensity vs. voltage for four analyzing polarizer angles from A.

0 V and 4 V. The signal measured with the analyzer and calibrated photodetector was correlated with the applied voltage. The analyzer was rotated between 0° and 360° in 5° increments and the results are plotted in Fig. 2(a). The peak of each trace was found in order to determine the peak-to-peak voltage that produces each polarization angle. The peak intensity value for each polarization angle was recorded so that the excitation power as a function of polarization angle could be determined. The differences in excitation power detected as a function of polarization angle result in part due to elements such as dichroic beam splitters in the optical path. These elements transmit different polarization angles with different efficiencies and can alter the polarization properties of the light as it enters the sample. Four of the calibration curves are plotted in Fig. 2(b) with the analyzer set to 0° , 45° , 90° , and 135° (equivalent to -45°). Though the curve for 0° is perpendicular to that for 90° , it possesses lower peak intensity due to the different transmission characteristics for that polarization in the excitation path. Note that the curve for the 45° analyzer in Fig. 2(b), corresponding to the tenth column of pixels in Fig. 2(a), shows higher intensity than its neighboring columns. This is a reproducible characteristic of our experimental setup. To achieve reasonable excitation efficiency for both DiI and Bodipy dyes at the same time, 488 nm laser light was used for excitation, but the LCVR in use is optimized for 532 nm excitation. The calibration reveals that the light is not perfectly linearly polarized but mixed with polarization states at other angles. It is shown later that our algorithm takes care of this artifact and yields the correct linear polarization response of the sample.

This necessitates the calculation of an intensity correction factor as a function of the rotated angle, from data similar to that shown in Fig. 4, to correct for non-uniform excitation powers and to enable quantitative measurements. Similarly, the polarized light incident at the sample may not be pure linear polarized light but be elliptical polarized light. Nevertheless, the linear polarization characteristics of the light have been determined through the instrument calibration process for each square wave applied voltage. This instrument cal-

ibration contains sufficient information to correct for either elliptical or partially polarized light, in order to calculate the sample's response to linear polarized light.

The linear polarization response as a function of the applied peak-to-peak voltage is saved as a calibration text file that is loaded into the PROM software written in LabVIEW. The polarization angles, to be used in the experiment, are chosen and the correct peak-to-peak voltage is found through interpolation of the calibration text file. The polarization angle referred to here is for the voltage that produces a maximum in intensity for a given polarization analyzer angle used during the calibration process. The polarization angles of the LCVR does not necessarily linearly correspond to those of the polarized light, but the data analysis does correct for this. The duration of each polarization angle is controlled through the software and there is synchronization with an Andor iXon EMCCD camera (Belfast, Northern Ireland), where LabVIEW is used to trigger the acquisition of the image frame by sending a transistor-transistor logic (TTL) pulse to the camera directly. The imaging integration time used in this study is 50 ms per frame.

B. Data analysis

This technique relies on measuring the differences in the emitted fluorescence of the dye molecules for different linear polarization states of light, based on the 2D projected angle that the absorption dipole of the dye molecule makes with the direction of polarization of the incident light. Measured fluctuations from other sources need to be taken into account so that the correct polarization properties can be assigned to each pixel in the image. An intensity calibration curve may be used to correct for differences in the intensity at different polarization angles, but it will not account for fluctuating light sources, which may be encountered if an unstable lamp is used. Another method, used in this paper, is to measure the average background autofluorescence from a region on the coverslip, or another marker, for use as an intensity reference for 10 mW incident laser power at 488 nm. The

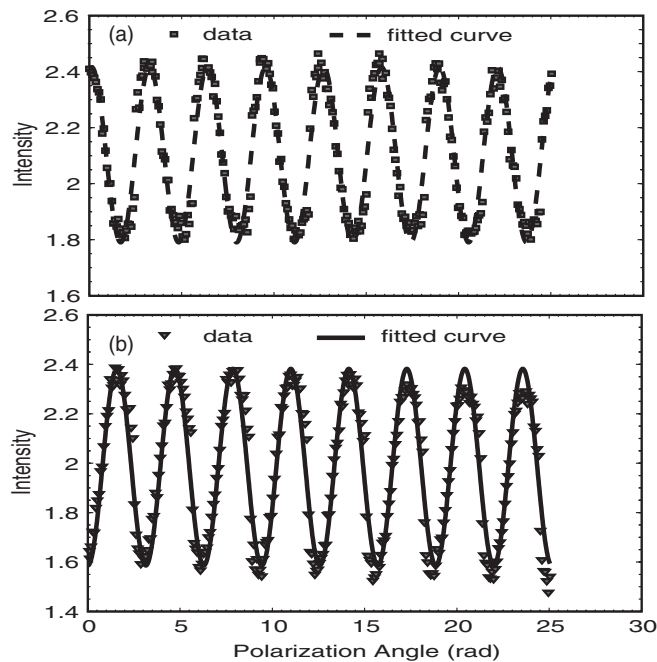


FIG. 3. Plots showing the collected fluorescence intensity for two different locations on the CA46 cell membrane labeled with DiI-PC. The polarization state of the excitation light was rotated between 0° and 180° in a 5° increment. The emitted fluorescence signal agrees well with a cosine squared fit shown as a red line. The offset of the cosine square function should theoretically agree with the average dipolar orientation. If the fit and the data points are closely examined, there are systematic deviations from the ideal cosine squared behavior. These deviations most likely arise from residual ellipticity in the polarization state of the light, and are a justification for the need of a calibration procedure to provide quantitative results. (a) The fluorescence intensity (units normalized by the background reference signal) of the location between the dipoles identified as 6 and 7 of the DiI labeled CA46 cell in Fig. 6(b). (b) The fluorescence intensity (arbitrary units) of the location marked by dipole number 1 of the DiI labeled CA46 cell in Fig. 6(b).

image frames are then normalized for 10 mW total excitation power into the objective by multiplying by the ratios of the background signal for each image to the reference background signal. The first, 0° , polarization image is taken as the 10 mW reference and the subsequent image frames are normalized to this value of excitation. The 0° polarization refers to the point in the calibration map where there is a correspondence between the applied voltage and a peak at 0° . Single dye molecules can show a triplet state saturation where the number of emitted photons deviates from a linear relationship with the incident laser power. One assumption in this analysis is that the fluorescence signal changes approximately linearly with changing incident light powers; this is reasonable, given the lower excitation powers densities and the higher labeling concentrations used in this study, which avoids the triplet state saturation regime.

As previously mentioned, three polarization states of light can be used to determine the average fluorescent dipole orientations in the presence of a spatially varying dc offset or background. By examining the fluorescence signal at individual pixels as a function of the linear polarization angle, the detected light can be fit to a cosine square function as is shown in Figs. 3(a) and 3(b). However, the fitting is algorithmically expensive and time consuming so it is not suited for calculating the average dipole angle for each pixel in an image

or movie in real-time. Using only the necessary and sufficient number of image frames to recover the polarimetric properties of the entire image allows for the study of faster dynamics of the fluctuation in the dipole orientation of dyes.

Using Stokes polarimetry, in the case where polarized light is incident at the sample and the light collected at the detector is not analyzed with a polarizer, it is possible to recover the polarized absorption properties of the sample. The Stokes parameters fully describe the polarization state of the incident light. There are four components with I being defined as the total intensity, Q being the difference between the amount of polarized light at 0° and that at 90° , U being the difference between the amount of polarized light at 45° and that at -45° , and with V being the difference between the amount of right-handed circular polarized light and the amount of left-handed circular polarized light. I here is normalized to unity. For polarized light, it is related to the polarimetric Stokes parameters through the equation

$$I^2 = Q^2 + U^2 + V^2. \quad (1)$$

The variables I , Q , and U can be measured through the calibration process, so it is straightforward to calculate the magnitude of V . For this analysis, we may also include possible contributions from unpolarized light into the V term because we are presently only concerned with the response of the sample to the Q and U components for linear polarized light. Knowing the difference between the amounts of linear polarized light versus the total light intensity is required to quantitatively determine the DOLE. The components from either circularly polarized or unpolarized light that contribute to the experimentally collected images will be accounted for because of the characterization of the Stokes parameters. The Mueller matrix can describe the interaction of a sample with an incident polarization characterized by the Stokes parameters. The Mueller matrix elements that we wish to find are the F_{11} , F_{12} , and F_{13} components. The F_{11} component is simply the fluorescence intensity image for a sample illuminated with unpolarized light. The F_{12} component is found by first collecting an image with an incident polarization at 0° and then collecting an image with the incident polarization rotated to 90° . The F_{12} component is formed then by subtracting the 90° image pixel-by-pixel from the 0° image. The F_{13} component is formed in a similar way but the images are first collected at 45° and -45° . Then the -45° image is subtracted from the 45° image pixel-by-pixel. These mathematical operations are depicted in Table I,

$$F_{11} = I_0 + I_{90} = I_{45} + I_{-45}, \quad (2)$$

$$F_{12} = I_0 - I_{90}, \quad (3)$$

$$F_{13} = I_{45} - I_{-45}, \quad (4)$$

where I_{angle} represents the fluorescence intensity collected for an incident linear polarization rotated to a specific angle. I_0 is defined as the detected fluorescence intensity for the Q Stokes parameter being equal to 1 or for perfectly incident 0° polarized light. These Mueller matrix components are not independent because either pair of crossed incident polarization angles can be used to measure F_{11} . This means three incident polarized intensities of light are sufficient to recover

TABLE I. The dumbbells represent the 2D orientations of single dye molecules with the rotation angle denoted at the right of the table. The 0, 45, 90 and -45° polarization signals represent incident light polarized at those angles. The relative polarized intensity (normalized to a maximum value of 1) collected from the fluorescent molecule depends on the angle between the molecule and the polarized light as $\cos^2(\delta - \theta)$ where δ represents the polarization angle of light and θ represents the 2D molecular orientation. The Mueller matrix components for the excitation of fluorescence with linear polarized light, the DOLE, and the rotation angle are found by combining the detected fluorescent intensities of the rotated molecules with different polarizations algebraically. If multiple molecules are present in a region or if the molecule rotates during the collection time, the time integrated signal can be used to measure the linear polarization response of the sample as is shown schematically with the samples with two dumbbells.

	I_0	I_{45}	I_{90}	I_{-45}	F_{11}	F_{12}	F_{13}	DOLE	ANGLE	
2D Molecular Orientation (deg) Emitted Fluorescence Intensity										0°
	1	0.5	0	0.5	1	1	0	1		45°
	0.5	1	0.5	0	1	0	1	1		67.5°
	0.146	0.854	0.854	0.146	1	-0.707	0.707	1		67.5°
2D Molecular Orientation (deg) Emitted Fluorescence Intensity										0°
	1.5	1.5	0.5	0.5	-2	-1	-1	0.707		45°
Signal					I_0 I_{45} + or + I_{90} I_{-45}	I_0 - I_{45} - I_{90} I_{-45}	I_{45} - I_{90} I_{-45}	$(F_{12}^2 + F_{13}^2)^{0.5}$ / F_{11}	$0.5 \tan^{-1} \left(\frac{F_{13}}{F_{12}} \right)$	0° $+ 90^\circ$
	0°	45°	90°	-45°					NA	

these sample parameters and one of the intensities may be discarded.

Since the actual experiment can contain incident light that does not possess perfect linearly polarized light at the angles we desire, we decided to recover the previously mentioned Mueller matrix parameters using an algebraic recovery. The detected fluorescence is now represented in the order of its collection, with the associated Stokes parameters of the incident light tagged to it. The total detected fluorescence, F_A , for a given incident full or partially linear polarized beam of light with Stokes parameters denoted by A is

$$F_A = F_{11}I_A + F_{12}Q_A + F_{13}U_A = F_{11} + F_{12}Q_A + F_{13}U_A. \quad (5)$$

The Stokes parameters for I are defined to be 1 and this represents the same total incident intensity that needs to be referenced for each incident polarized light beam. In order to solve for these three Mueller matrix parameters, F_{11} , F_{12} , F_{13} , we need to supply three equations. This is accomplished by illuminating the sample with three different beams with different Stokes parameters. The more distinct the different incident polarizations are, the better the recovery will be. The additional equations are defined as

$$F_B = F_{11}I_B + F_{12}Q_B + F_{13}U_B = F_{11} + F_{12}Q_B + F_{13}U_B, \quad (6)$$

$$F_C = F_{11}I_C + F_{12}Q_C + F_{13}U_C = F_{11} + F_{12}Q_C + F_{13}U_C. \quad (7)$$

Using these equations we first solve for F_{13} ,

$$F_{13} = \frac{F_A(Q_C - Q_B) + F_B(Q_A - Q_C) + F_C(Q_B - Q_A)}{Q_C(U_A - U_B) + Q_B(U_C - U_A) + Q_A(U_B - U_C)}. \quad (8)$$

Next, we use the results from F_{13} and the three experimental measurements to solve for F_{12}

$$F_{12} = \frac{1}{2} \left(\frac{F_A - F_B}{Q_A - Q_B} + \frac{F_C - F_B}{Q_C - Q_B} - F_{13} \left[\frac{U_A - U_B}{Q_A - Q_B} + \frac{U_C - U_B}{Q_C - Q_B} \right] \right), \quad (9)$$

and finally we solve for F_{11} using the previous results

$$F_{11} = \frac{1}{3} (F_A + F_B + F_C - F_{12}(Q_A + Q_B + Q_C) - F_{13}(U_A + U_B + U_C)). \quad (10)$$

We now have the results that provide for the unpolarized intensity image, F_{11} , and the polarization difference images discussed in the introduction F_{12} and F_{13} . These results can now be used to find the rotation invariant DOLE,

$$DOLE = \frac{\sqrt{F_{12}^2 + F_{13}^2}}{F_{11}}, \quad (11)$$

and the net rotation angle for the excitation of the fluorescence θ ,

$$\theta = \frac{1}{2} \tan^{-1} \left(\frac{F_{13}}{F_{12}} \right). \quad (12)$$

C. Cell preparation and fluorescent labeling

CA46 cells were maintained in Roswell Park Memorial Institute medium without phenol red, supplemented with 10% fetal bovine serum, 200 units/ml penicillin, and 200 $\mu\text{g}/\text{ml}$ streptomycin at 37°C in a humidified 5% CO_2 atmosphere. For labeling, a cell pellet (1×10^6 cells) was resuspended in a dye solution (0.5 μM –5 μM DiI or Bodipy in $1 \times$ phosphate buffered saline solution) and incubated at 37°C for 10 min, then the labeled cells were washed with cell growth medium twice to remove free dye molecules. For imaging, the labeled cells in cell growth medium were transferred to a small polydimethylsiloxane (PDMS) chamber bottomed with a coverslip. The PDMS chamber was sealed with a microscope slide to prevent solution evaporation. All cell culture reagents were purchased from Invitrogen (Carlsbad, CA).

III. RESULTS

The calibrated polarization rotator was used to excite a single DiI-labeled CA46 cell. The results that are presented in Fig. 4 are images of polarization-dependent DiI fluorescence emission for a simulated DiI-labeled spherical liposome and a typical CA46 cell. In a simulated liposome, DiI molecules are homogeneously distributed along the membrane with their absorption dipoles tangential to the membrane curvature so that the polarization dependency arises from the orientations of the DiI molecules associated with the membrane curvature.

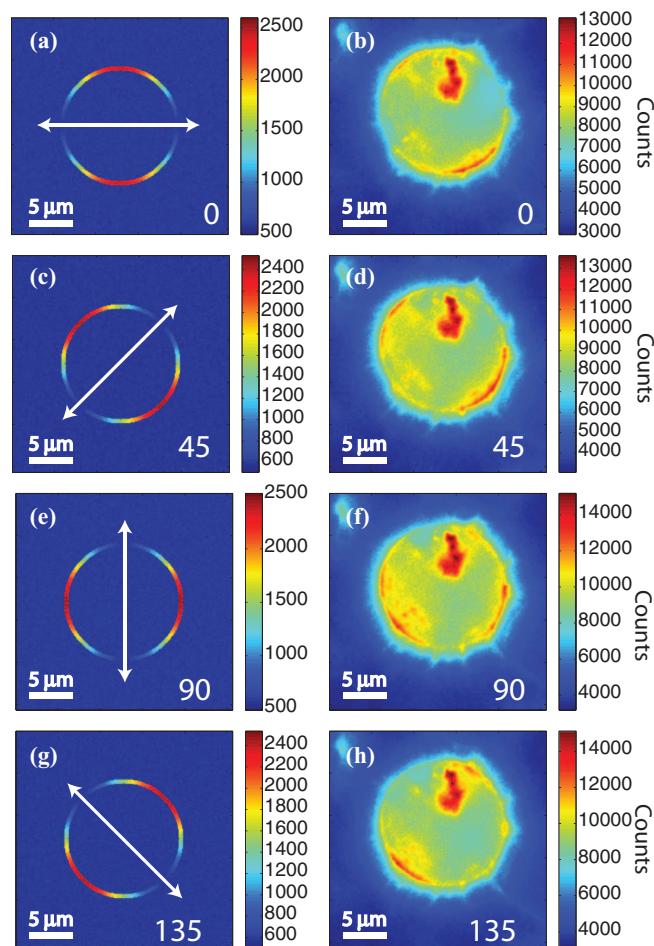


FIG. 4. DiI molecules, which lie tangential to the membrane surface, are excited optimally when the polarization angle (indicated by the arrows) is aligned with the absorption dipoles of the DiI dyes. The panels in the left column ((a), (c), (e), and (g)) represent a simulation of DiI molecules oriented tangentially to the membrane of a circular liposome. The emission of fluorescence is proportional to the angle between the polarization of the incident light and the orientation of the DiI absorption dipole. The panels in the right column ((b), (d), (f), and (h)) represent the detected fluorescence from a typical single CA46 cell labeled with DiI-PC. There is a general agreement with the simulated data. However, the DiI dye distribution is non-uniform in the CA46 cell, affecting the fluorescence distribution. The polarizations in the CA46 images represent the polarized beams shown in Fig. 2(b). As such they need to be corrected for incident elliptical polarized light by using the Stokes parameters for the light characterized at those analyzer angles.

As expected, the left panels for the simulated liposome represent the detected fluorescence emission based on the angle between their absorption dipoles and the angle of pure linearly polarized light. The corresponding images for the CA46 DiI labeled cells at the same angle are compared next to the simulated images. The polarized light angles used to excite the DiI molecules in the CA46 cell are identical to those in Fig. 2. The intensity pattern for the CA46 cells qualitatively agrees with the expected distribution pattern of the simulated images. In reality, the actual density of DiI molecules in the cell membrane is nonuniform because of the formation of lipid domains, and the incident light used for these images was not purely linearly polarized light, so the Stokes parameters were measured for the incident light.

The differences in local lipid concentrations, caused by the lipid domains, leads to a spatially varying fluorescence in-

tensity signal that contains additional information about the organization of lipid molecules in the cell membrane. There is also labeling of internal cellular structures with the DiI-labeled lipids, which may provide information about the trafficking of lipid molecules in and out of the cell. The images shown in Fig. 4 contain all the information necessary to determine the linear polarization response of the DiI molecules in the plasma membrane as well as inside the cell. Although only three of these images would be sufficient for this analysis, four are included to reduce the uncertainty involving compressed sampling. The improvement is achieved by processing each set of three images out of four obtained at four different polarization angles. These four sets of data are then averaged together to reduce sampling uncertainties.

The images of Fig. 4 can be combined to find the polarization response Mueller matrix elements, F_{11} , F_{12} , and F_{13} , for each pixel in the image. The simulated DiI-PC labeled liposome image is compared with the CA46 cell to analyze the dipole orientation of DiI molecules in the cell. The liposome images are calculated by Eqs. (2)–(4), used for pure linear polarized light, where the images are either added or subtracted. The corresponding Muller matrix images for the CA46 cells were calculated using the full matrix algebra applied to the experimentally determined Stokes parameters of the incident light. Again, three images at three incident polarization angle are sufficient for the analysis, but the four images from Fig. 4 were taken in sets of 3 to determine F_{11} , F_{12} , F_{13} using Eqs. (8)–(10) (see supplementary material). The four images were divided into four sets of three, the results determined and then averaged. Even though the F_{11} intensity distribution was not uniform for the CA46 cell, the F_{12} and F_{13} distributions agree well with the expected distribution shown in the simulated sample. There is a slight rotation in the experimental sample relative to the simulation, due to the analyzing polarizer being rotated 2.5° in its rotation mount. This 2.5° rotation is in agreement with the measured rotated angles and is subsequently subtracted from the rotated angle image.

These Mueller matrix images, shown in Fig. 5, can then be used to calculate DOLE images (Eq. (11)) and angular orientation images (Eq. (12)), and the results are shown in Fig. 6. The DOLE image of simulated liposome shows an expected uniform intensity along the membrane. The simulated angular image shows that the orientation angle wraps between 0° and 180° indicative of well-defined dipole orientations tangential to the membrane curvature. The DOLE image for the CA46 cell shows a ring around the cell membrane. This indicates that the dye molecules in the cell membrane within the optical section exhibit a net linear orientation tangential to the membrane. On the other hand, the internally labeled cellular structures do not exhibit this net linear orientation over the time scale of the measurement, resulting in zero DOLE signal. The DOLE signal is used here simply for additional image contrast to show the response to linear polarized excitation light. A background subtraction for the points with significant DOLE signal can be used to more accurately measure the DOLE signal. If the signal is background corrected, the DOLE image will possess errors because there will be a division by zero or negative numbers in the regions of the

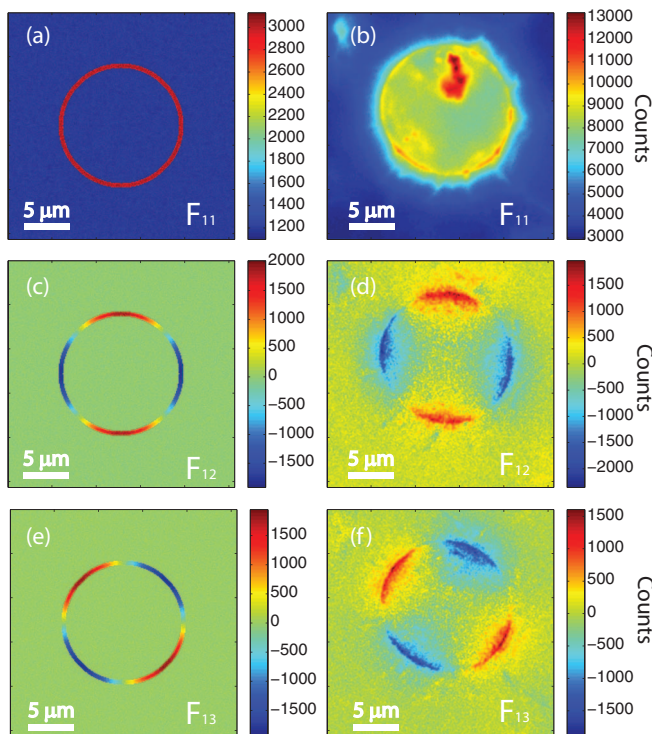


FIG. 5. Mueller matrix parameter images of a simulated liposome and a real CA46 cell labeled with DiI-PC molecules. The left column represents the simulated DiI-PC labeled liposome from Fig. 4 using the simple calculations possible with perfect linear polarized light. The right column represents the algebraically reconstructed Mueller matrix parameters. (a) The F_{11} intensity image calculated from either Fig. 4(a) plus Fig. 4(c) or Fig. 4(c) plus Fig. 4(g). (b) The F_{11} image for the CA46 cell calculated with the algebraic reconstruction. (c) The F_{12} image for the simulated liposome showing the difference in response to 0° and 90° polarized light. (d) The F_{12} image for the CA46 cell showing the difference in response to 0° and 90° pure polarized light. (e) The F_{13} image for the simulated liposome showing the difference in response to 45° and -45° polarized light. (f) The F_{13} image for the CA46 cell showing the difference in response to 45° and -45° pure polarized light.

image where there is background only. This background will be present only in the F_{11} image.

The F_{12} and F_{13} images are automatically corrected for background because they are difference images. The angular orientation image is also automatically background corrected. Also, presented in the CA46 DOLE image is the measured angular orientation of the cell membrane at different points wrapping around the cell membrane. The results are consistent with DiI laying tangential to the cell membrane. The corresponding angular orientation image in Fig. 6(d) shows the orientation of DiI in the membrane for each point in the image. It is noteworthy that this image was constructed from the DOLE image because it provides meaningful data only when the DOLE signal is non-zero. Therefore, even if there is a correlation in the angular orientation image, those data points may possess mathematical errors attributed to zero-valued DOLE signal. Further investigations will explore the propagation of uncertainties due to photon counting in these types of ratiometric measurements. This may be useful for assigning uncertainties to both the angular and DOLE values calculated for each image pixel. Probability theory approaches to data analysis may also correct for the problems

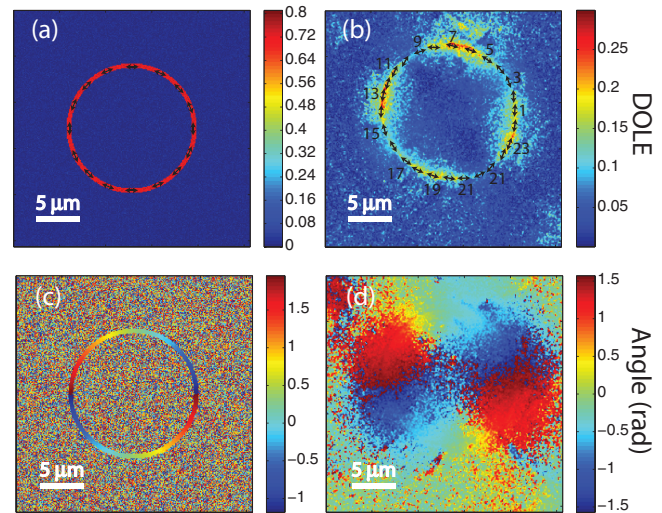


FIG. 6. (a) The DOLE image for the simulated circular liposome with tangentially aligned DiI molecules. The double arrows represent the DiI dipole orientation and the angles were taken from panel (c). (b) The experimentally measured DOLE image for the CA46 cell. The cell membrane shows DOLE contrast whereas the internal cellular structures show no change with linear polarization and have zero DOLE signal. Dipoles represented as double arrows are plotted along the cell membrane and the orientations were taken from panel (d). (c) The angular orientation image for the simulated liposome image. The corresponding areas where the DOLE signal is zero due to ensemble averaged fluorescence emission from multiple dyes with randomized orientations. (d) The angular orientation image for the CA46 cell. The net orientation angles can be taken from the regions where the DOLE is non-zero.

associated with background subtraction that can lead to errors in forming the DOLE images.

IV. DISCUSSION

We have shown that a low cost, liquid crystal polarization rotator can be used to sweep through a range of polarization angles using simple signal generation equipment. The minimum switching time of the liquid crystal is on the order of 20 ms while the polarization angle can be maintained for an arbitrary time period. In addition, the image acquisition can be easily synchronized with the polarization angle (Stokes parameters). Our scheme allows a 2D projection of the polarization angle to be calculated from the detected fluorescence signal at each point in the image. The polarization modulation also allows for the background free detection and calculation of F_{12} , F_{13} , and angular orientation images. The higher labeling densities in these measurements allow the diffraction-limited, average dye angles to be measured in a full-field image in the two dimensions of the optical slice. Under the far-field illumination in our current microscopy configuration, Bodipy-labeled cells do not show polarization state-dependent emission intensity whereas DiI labeled membranes do. The results on Bodipy-labeled cells are included in the supplementary material. This provides evidence that the polarization state-dependency we observed is mainly due to the orientation of the absorption dipole of dye molecules.

Our method has significant advantages over other schemes that have been used to perform polarization measurements. For example, polarization rotation using a photoelastic modulator offers a signal-to-noise advantage over other

techniques because it involves high frequency modulation and can be combined with a lock-in amplifier to detect a signal at the same modulation frequency.²⁰ However, although this technique is useful for raster scanning an image, the modulation frequency is too fast to perform wide-field imaging with an EMCCD camera. Single molecule techniques also are capable of determining the absorption dipole orientations through excitation patterns,²¹ direct emission pattern imaging,²² recording aberrated²³ or defocused images,²⁴ or sophisticated analysis based on the signal from multiple photodetectors.²⁵ Yet, for samples with high dye densities that do not allow single molecules to be resolved, these techniques become limited or impractical. Also, total internal reflection (TIR) approaches have been employed to determine dye orientations near substrates,²⁶ but the TIR technique is limited to axial depths on the order of a couple hundred nanometers since the excitation field decays exponentially as a function of distance from the substrate surface. Two photon microscopy has also been combined with polarization based excitation imaging,²⁷ but this complementary technique requires raster scanning of the focused laser beam which limits the image acquisition speed.

Future modifications of the scheme discussed in this paper could allow 3D mapping of the amplitude and the average dipole orientation angle in cell membranes. This can be accomplished by translation of the microscope objective in the axial direction. Also, tilting of the optical sections could allow for the 2D dye orientations images to be reconstructed into a 3D image. Labeling head groups with dyes with different emission spectra (e.g., DiI), that have different length acyl chains attached, will allow membrane surface structure to be associated with the presence of membrane microdomains through the F_{11} intensity images. Labeling different length acyl chains with differently colored dyes, similar to Bodipy at different points on one of the two acyl chains, will allow for the determination of the acyl chain structure that can be correlated with the microdomain information. Bodipy groups on molecules labeled closer to the head group would be expected to be more rigid compared to those on molecules labeled further along their acyl chains. The image processing is matrix based, so the calculation of the experimental parameters is efficient and should be well suited to real-time image processing and data display. The combination of a careful calibration of the polarization states of different colors of light transmitted through a LCVR can also be combined with this algorithm to extend this method to multispectral or hyperspectral studies. Because of the simplicity of this instrument and the ability to externally couple any illumination source for a variety of imaging platforms, this technique could be adapted to find broad applications such as the study of membrane mechanics and membrane structural biology in microscopy, and polarimetric imaging of tissues and organs with *in vivo*, real-time endoscopy.

ACKNOWLEDGMENTS

The authors thank Dr. Maritoni Litorja, Dr. David Allen, Dr. Eric Shirley, and Dr. Kimberly Briggman at National In-

stitute of Standards and Technology (NIST) and Fuyuki Tokumasu at National Institute of Allergy and Infectious Diseases of the National Institutes of Health (NIH) for helpful discussions and suggestions. This research was supported by NIST Innovative Measurement Science program on optical medical imaging. This research was performed while J.L. and J.R.K. held National Research Council Research Associateships supported by NIH (NIBIB)/NIST. Funding for these awards was provided by the intramural program of the National Institute for Biomedical Imaging and Bioengineering of the NIH. J.F.L. held a National Research Council Research Associateship supported by NIST. D.S. and R.N. were supported by intramural funds of the *Eunice Kennedy Shriver* National Institute of Child Health and Human Development, NIH. Certain commercial equipment, instruments, or materials are identified in this paper. Such identification does not imply recommendation or endorsement by the National Institute of Standards and Technology, nor does it imply that the materials and instruments are necessarily the best available for the purpose.

- ¹J. Chung, W. Jung, M. J. Hammer-Wilson, P. Wilder-Smith, and Z. Chen, *Appl. Opt.* **46**, 3038 (2007).
- ²V. Backman, R. Gurjar, K. Badizadegan, I. Itzkan, R. R. Dasari, L. T. Perelman, and M. S. Feld, *IEEE J. Sel. Top. Quantum Electron.* **5**, 1019 (1999).
- ³I. H. Shin and D. Y. Kim, *J. Biomed. Opt.* **15**, 016028 (2010).
- ⁴A. N. Yaroslavsky, V. Neel, and R. R. Anderson, *Opt. Lett.* **29**, 2010 (2004).
- ⁵G. J. Schütz, G. Kada, V. P. Pastushenko, and H. Schindler, *EMBO J.* **19**, 892 (2000).
- ⁶M. G. Ismail, *et al.*, *Hepatology* **49**, 1673 (2009).
- ⁷S. Charrin, F. Naour, O. Silvie, P. E. Milhiet, C. Boucheix, and E. Rubinstein, *Biochem. J.* **420**, 133 (2009).
- ⁸A. K. Neumann, M. S. Itano, and K. Jacobson, *F1000 Biol Rep.* **2**, 31 (2010).
- ⁹A. Kress, P. Ferrand, H. Rigneault, T. Trombik, H. T. He, D. Marguet, and S. Brasselet, *Biophys. J.* **20**, 468 (2011).
- ¹⁰D. Axelrod, *Biophys. J.* **26**, 557 (1979).
- ¹¹H. S. Muddana, R. R. Gullapalli, E. Manias, and P. J. Butler, *Phys. Chem. Chem. Phys.* **13**, 1368 (2011).
- ¹²P. W. Livanec and R. C. Dunn, *Langmuir* **28**, 14066 (2008).
- ¹³W. C. Wimley and T. E. Thompson, *Biochemistry* **29**, 1296 (1990).
- ¹⁴J. Korlach, P. Schwille, W. W. Webb, and G. W. Feigensohn, *Proc. Natl. Acad. Sci. U.S.A.* **96**, 8461 (1999).
- ¹⁵J. Hwang, L. K. Tamm, C. Bohm, T. S. Ramalingam, E. Betzig, and M. Edidin, *Science* **270**, 610 (1995).
- ¹⁶J. Rieppo, J. Hallikainen, J. Jurvelin, I. Kiviranta, H. J. Helminen, and M. Hyttinen, *Microsc. Res. Tech.* **71**, 279 (2008).
- ¹⁷See supplementary material at <http://dx.doi.org/10.1063/1.4717682> for the experimental results for Bodipy-PC labeled CA46 cells.
- ¹⁸J. Y. Lee, Ji Youn Lee, J. F. Lesoine, J. R. Krogmeier, H. Kang, M. Clarke, R. Chang, D. L. Sackett, R. Nossal, and J. C. Hwang, *Proc. SPIE* **7891**, 78910Z-1 (2011).
- ¹⁹T. C. Larson and J. M. Houston, NIST Special Pub. 250-41 (2008); <http://www.nist.gov/calibrations/upload/sp250-41a.pdf>.
- ²⁰K. W. Hipps and G. A. Crosby, *J. Phys. Chem.* **83**, 555 (1979).
- ²¹L. Novotny, M. R. Beversluis, K. S. Youngworth, and T. G. Brown, *Phys. Rev. Lett.* **86**, 5251 (2001).
- ²²M. A. Lieb, J. M. Zavislan, and L. Novotny, *J. Opt. Soc. Am. B* **21**, 1210 (2004).
- ²³A. P. Bartko and R. M. Dickson, *J. Phys. Chem. B* **103**, 3053 (1999).
- ²⁴A. P. Bartko and R. M. Dickson, *J. Phys. Chem. B* **103**, 11237 (1999).
- ²⁵J. T. Fourkas, *Opt. Lett.* **26**, 212 (2001).
- ²⁶A. Anantharam, B. Onoa, R. H. Edwards, R. W. Holz, and D. Axelrod, *J. Cell Biol.* **188**, 415 (2010).
- ²⁷A. Gasecka, T. Han, C. Favard, B. R. Cho, and S. Brasselet, *Biophys. J.* **97**, 2854 (2009).